FIBER OPTIC COMPARED TO RING LASER OPTICAL GYROS

Paul G. Savage
Strapdown Associates, Inc.
Maple Plain, MN 55359 USA

WBN-14034
www.strapdowassociates.com
April 22, 2024

ABSTRACT

Fiber optic and ring laser gyros (FOGs and RLGs) create counter-travelling monochromatic light waves in a closed optical path to measure angular rate around an axis perpendicular to the wave path. This article addresses the similarities and differences between FOGs and RLGs, showing that they both emanate from the same analytical expression. A FOG creates the closed wave path using an optical fiber coil; the optical source is a super luminescent diode residing within the gyro, but external to the coil. Light waves traverse the coil length once when their combined amplitude is detected to measure angular rotation over the time for the beams to traverse the fixed coil length. For an RLG, the wave path is created by reflecting mirrors surrounding a closed cavity in which laser generated light resides. Light amplification by the laser stimulated emission process creates and sustains the continuous counter-travelling light beams that originate at laser ignition. The result is a continually increasing path length for the counter-travelling beams, the optical readout measuring gyro angular rotation since ignition. This article describes the operation of FOGs and RLGs, then compares them analytically.

INTRODUCTION

Refs. [1] and [2] provide detailed analytical derivations describing the operation of optical gyros and how Relativity enables their ability to measure angular rotation. All optical gyros create closed optical paths housing counter-travelling monochromatic light waves. Ref. [1] is general for any wave path shape used for the counter-travelling waves. Ref. [2] is a simplified version of [1] in which the wave path is circular, corresponding to the equivalency shown in [1] between general wave path shapes and their circular equivalents. This article is a further extension of [2], based also on circular optical wave paths.

The difference between this article and [1] is on its emphasis in the similarities and differences between fiber optic and ring laser gyros (FOGs and RLGs) without dwelling on Relativistic and Euclidean kinematic predictions detailed in [1] and [2]. As in [1] and [2], derivations of gyro operation are carried out in rotating gyro space in which the readout and light source is located. As a result, the distance and travel time around the wave path is the same for each of the counter-rotating light beams. This contrasts with traditional optical gyro operation explanations, derived in non-rotating inertial space around which the gyro rotates. In non-

rotating space, the distance and time of travel between the counter-travelling waves differs, a characteristic ingrained in the minds of many optical gyro designers.

In this and the [1], [2] derivations, the effect of rotation is shown to shift the wavelength of the counter-travelling light beams, reducing it for the clockwise (cw) beam, increasing it for the counter-clockwise (ccw) beam. The wavelength difference creates a measureable effect at the gyro readout detectors where the light beams optically combine "interferometrically". For a FOG the path length is fixed, generating a fixed output for a given angular rate. For RLGs, angular rotation generates an increasing difference between the counter-travelling wave path lengths, creating a changing readout that measures fixed increments of accumulating rotation angle. This fundamental difference is caused in an RLG by the stimulated emission process within the laser that sustains energy in the counter-travelling light beams created at laser ignition. The result is the equivalent of a continually increasing light wave path length.

This article begins by first deriving the fundamental equation governing all optical gyros, showing how the light beam wavelengths are shifted by angular rotation, oppositely for cw compared with the ccw beams. It is then analytically demonstrated how the wavelength difference translates into a phase shift difference between the cw and ccw monochromatic light waves, the signal ultimately measured for output. Based on the derived fundamental equation of optical gyro operation, "open-loop" FOGs, "closed-loop" FOGs, and a representative RLG are then analytically described and compared, explaining the fundamental similarities and differences between the two optical gyro design approaches.

ANALYTICALLY DESCRIBING ALL OPTICAL GYROS

Consider two points *b* and *i*, *i* in linear motion relative to *b*. Also, consider two time instants t_1 and a short time later t_2 with the *i* location at these times designated as $i(t_1)$ and $i(t_2)$. Define points *i* and *b* to be coincident at t_1, with *i* displaced from *b* at t_2 by linear distance Δx_{bi} (from *b* to *i*). The geometry is depicted in Fig. 1.

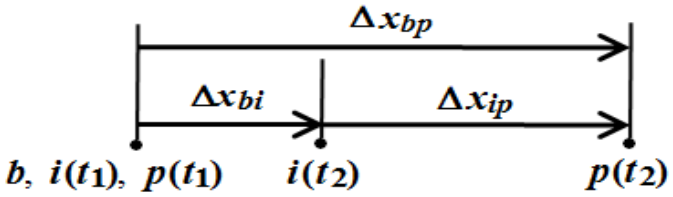

Fig. 1 Relative Motion Geometry

Now consider a photon of light designated as point *p*, travelling in the same direction as point *i*. Define *p* to be coincident with *i* and *b* at t_1 and displaced from both at time t_2. At t_2, define the distances between the points as Δx_{bp} (from *b* to *p*) and Δx_{ip} (from *i* to *p*) as shown in Fig. 1. In the figure, $p(t_1)$ and $p(t_2)$ designate the locations of *p* at times t_1 and t_2. Based on these definitions and those in the previous paragraph we can then write from Fig. 1:

$$\Delta x_{bp} = \Delta x_{bi} + \Delta x_{ip} \qquad (1)$$

When the velocity magnitude between observers is small compared to the speed of light, the observed motion forecasted by Special Relativity theory [3 Part 1; 4 Chpt VI; 5] reduces to (1), the classical Euclidean kinematic prediction [3 pp 37-38; 4 Chpt III Sect 7; 6 Sect 12-1].

Say that the Δx_{ip} measurement initiates when the leading edge of the *p* photon light wave passes point *i* and terminates when the leading edge of the next wave passes that point. Then Δx_{ip} will represent λ_{ip}, the wavelength of the *p* wave at point *i*. Substituting in (1) thereby finds with rearrangement:

$$\frac{\Delta x_{bp}}{\lambda_{ip}} = 1 + \frac{\Delta x_{bi}}{\Delta x_{ip}} \qquad (2)$$

Note from Fig. 1, however, that the Δx_{bp} measurement is independent of point *i* motion, hence, would be the same no matter what the value of Δx_{bi}. Thus, if we define λ_{0_p} as the value of λ_{ip} under zero *i* motion relative to *b* (i.e., zero Δx_{bi}), we see from (2) that $\Delta x_{bp} = \lambda_{0_p}$, and (2) becomes

$$\frac{\lambda_{0_p}}{\lambda_{ip}} = 1 + \frac{\Delta x_{bi}}{\Delta x_{ip}} \qquad (3)$$

Application To Optical Gyros

Optical gyros contain a closed wave path through which correlated light is simultaneously circulated in two directions, "clockwise" (cw) and "counterclockwise" (ccw), around a central point *a* fixed in the gyro. For this discussion, we will consider the wave path to be circular. Ref. [1] show that for a regular polygon shaped wave path, equivalent performance would be achieved for a circular wave path having a radius equal to that of a circle that can be inscribed within the polygon.

Define points *b*, *i*, and *p* to be located in the wave path with *p* in (1) representing a photon in the cw light wave, *i* representing a point attached to the rotating gyro, and *b* being at the end-point of an inertially non-rotating line from central point *a* to point *b*. Fig. 2 depicts the relative photon position motion along the light wave path enclosed within an optical gyro. As the gyro rotates in Fig. 2 through small inertial angular increment $\Delta\theta$, point *i* will translate around point *a* as $\Delta x_{bi} = r\Delta\theta$ where *r* is the radius of the gyro circular wave path. Thus, (3) becomes

$$\frac{\lambda_{0_p}}{\lambda_{ip}} = 1 + \frac{r\Delta\theta}{\Delta x_{ip}} \qquad (4)$$

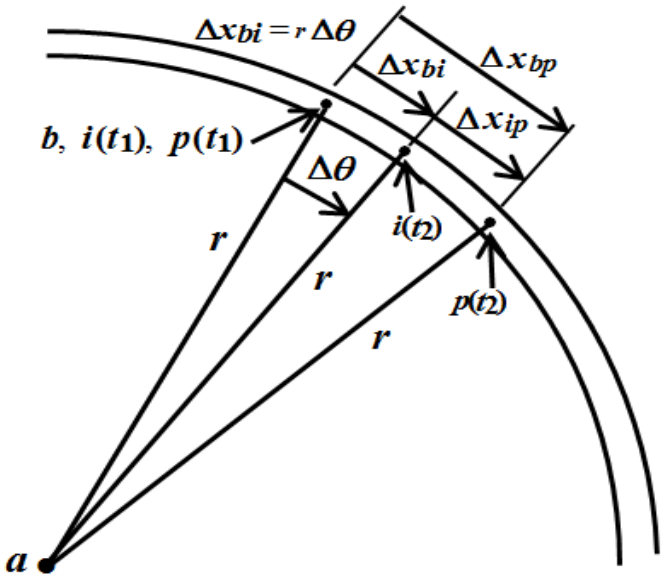

Fig. 2 Position Changes Along The Wave Path

The Effect Of Relativity

The basic precept of Relativity theory is that the speed of light is the same constant c when measured in any moving coordinate frame [5; 7 Appendix A]. In (4), Δx_{ip} is the change in photon position that would be measured at moving point i within the gyro wave path. If we define small time interval Δt (measured on a point i located clock) for a Δx_{ip} (and $\Delta\theta$) measurement to occur, the equivalent photon velocity would be $V_{ip} = \Delta x_{ip} / \Delta t$, or $\Delta x_{ip} = V_{ip}\,\Delta t$. However, since p is a photon of light, V_{ip} also represents the velocity of light measured at moving point i. But from Relativity theory, $V_{ip} = c$ so that $\Delta x_{ip} = c\Delta t$. We can also define the gyro measured angular rate ω relative to non-rotating inertial space as $\omega = \Delta\theta / \Delta t$, or $\Delta\theta = \omega\Delta t$. Substituting for Δx_{ip} and $\Delta\theta$ in (4) then obtains

$$\frac{\lambda_{0_p}}{\lambda_{ip}} = 1 + \frac{r\,\omega\Delta t}{c\Delta t} = 1 + \frac{r}{c}\omega \qquad (5)$$

The Rotation Effect On The Oppositely Travelling Light Waves

Thus far, we have only accounted for the effect of rotation on the cw (clockwise) p wave travelling in the closed gyro wave path. A similar result applies for a ccw (counterclockwise) travelling q wave photon. However, because the q wave is moving oppositely from the p wave direction, the effect of ω angular rotation will be in the opposite direction. Thus, the equivalent of (5) for a q wave photon would be

$$\frac{\lambda_{0_q}}{\lambda_{jq}} = 1 - \frac{r}{c}\omega \qquad (6)$$

In (6), subscript *q* refers to the oppositely travelling *q* wave photon and *j* refers to the location of the *q* photon in the gyro wave path, generally at a different point than the *i* location for the *p* photon.

Ref. [1] shows that for both fiber optic and ring laser optical gyros, the λ_{0_p}, λ_{0_q} wavelengths of the *p*, *q* waves under zero rotation will be the same, thus, we can dispense with the *p*, *q* designation and define the zero angular rate wavelength for both the cw and ccw waves as λ_0. Then (5) and (6) become

$$\frac{\lambda_0}{\lambda_{ip}} = 1 + \frac{r}{c}\omega \qquad \frac{\lambda_0}{\lambda_{jq}} = 1 - \frac{r}{c}\omega \qquad (7)$$

Wave Height Measurement For Readout

To understand how an optical gyro uses (7) to measure angular rate, consider that the wave path followed by each *p* and *q* light wave photon ends in the gyro "readout zone", and at an earlier time, each photon entered (or originated in) the wave path in the same readout zone. (Note, depending on the gyro configuration, the phase of the *p* or *q* wave photons may differ at the point of "entry").

Consider now that each cw and ccw photon will traverse the same distance relative to the gyro during its time of travel from wave guide "entry" (in the readout zone) to its time of measurement (in the readout zone). Thus, the total distance travelled by each photon since wave guide entry will be the same total wave guide path length. (Note, depending on the gyro configuration, the wave path generally consists of a sequence of circular paths, sometimes overlapping, sometimes almost parallel, but interconnected.) Finally, since each photon traverses the same distance at the same speed of light, the time interval from wave path "entry" to measurement (in the readout zone) will be the same for the clockwise *p* as it is for the counter-clockwise *q* photons. This is a critical point because it has a direct impact on the ability to extract a measurement of gyro angular motion from the cw and ccw light waves when they optically combine in the readout zone – see further discussion following (13).

Based on the previous discussion, consider the clockwise *p* and counter-clockwise *q* wave photons at a particular instant of time. Assume that both photons entered (or originated) in the readout zone at an earlier time (as described in the previous paragraph), that the time interval for each photon to traverse the wave path since entry is *T*, and that each wave is sinusoidal at amplitude *B*. The wave heights $g(T)_p$, $g(T)_q$ at time *T* in the readout zone would then be

$$g(T)_p = B\sin\phi(T)_p \qquad g(T)_q = B\sin\phi(T)_q$$
$$\phi(T)_p = \phi_{0_p} + \Delta\phi(T)_p \qquad \phi(T)_q = \phi_{0_q} + \Delta\phi(T)_q \tag{8}$$

where $\phi(T)_p$, $\phi(T)_q$ are the readout wave phases at time *T*, the wave photon phases at readout zone entry are ϕ_{0_p}, ϕ_{0_q}, and $\Delta\phi(T)_p$, $\Delta\phi(T)_q$ are differences in readout zone wave photon phases at time interval *T* (i.e., since wave path entry).

At readout time instant *T*, a complete cw and ccw wave will exist in the waveguide and the phase for each since entry at each point in the wave will be a function of its *i, j* location history along the wave path as defined in (7). As each wave photon traverses its *i, j* position, (7) shows that the wavelength will depend on the ω angular rate at each *i, j* location. For temporary simplicity, we now consider the angular rate to be constant during time interval *T* so that (7) becomes independent of *i, j* location, simplifying to

$$\frac{\lambda_0}{\lambda_p} = 1 + \frac{r}{c}\omega \qquad \frac{\lambda_0}{\lambda_q} = 1 - \frac{r}{c}\omega \tag{9}$$

In (9), λ_p, λ_q are the *p, q* wavelengths at any *p, q* location under constant angular rate. At this same readout instant of time *T*, we can also write

$$\Delta\phi(T)_p = 2\pi\frac{L}{\lambda_p} \qquad \Delta\phi(T)_q = 2\pi\frac{L}{\lambda_q} \tag{10}$$

where *L* is the total wave path travel distance for each photon (from entry into the wave path readout zone to the time of readout in the readout zone). But since each wave travels at the speed of light *c*, wave path *L* also equates to *c T*. Thus, for constant angular rate ω, (8) with (9) and (10) becomes

$$g(T)_p = B\sin\left(\phi_{0_p} + 2\pi\frac{cT}{\lambda_q}\right) = B\sin\left[\phi_{0_p} + \frac{2\pi\, cT}{\lambda_0}\left(1 + \frac{r}{c}\omega\right)\right] = B\sin\left(\phi_{0_p} + \frac{2\pi\, cT}{\lambda_0} + \frac{2\pi r}{\lambda_0}\omega T\right)$$
$$g(T)_q = B\sin\left(\phi_{0_p} + 2\pi\frac{cT}{\lambda_q}\right) = B\sin\left[\phi_{0_p} + \frac{2\pi\, cT}{\lambda_0}\left(1 - \frac{r}{c}\omega\right)\right] = B\sin\left(\phi_{0_q} + \frac{2\pi\, cT}{\lambda_0} - \frac{2\pi r}{\lambda_0}\omega T\right) \tag{11}$$

Eqs. (A-5) and (A-6) in the Appendix show that under the more general conditions where ω is time varying, the ωT products in (11) represent the time integral of ω as the wave front travels in time from wave path entry to readout over time interval *T*. Then the more general form of (11) would be

$$g(T)_p = B\sin\left(\phi_{0_p} + \frac{2\pi\, cT}{\lambda_0} + \frac{2\pi r}{\lambda_0}\int_{\tau=0}^{\tau=T}\omega(\tau)\,d\tau\right)$$
$$g(T)_q = B\sin\left(\phi_{0_q} + \frac{2\pi\, cT}{\lambda_0} - \frac{2\pi r}{\lambda_0}\int_{\tau=0}^{\tau=T}\omega(\tau)\,d\tau\right) \qquad (12)$$

In (12), τ is the time interval from photon entry (or creation) to the time it moves over distance $c\,\tau$ along the wave path at the speed of light *c*, and $\omega(\tau)$ is time varying angular rate ω at time τ. The $g(T)_p$ and $g(T)_q$ wave signals in (12) optically combine in the readout zone ("interferometrically") for measurement on photo-diode optical detectors. The combined wave measurement determines the integrated angular rate $\int_{\tau=0}^{\tau=T}\omega(\tau)\,d\tau$ for optical gyro output.

Combined Oppositely Directed Waves In The Readout Zone

In the readout zone at time interval *T* (from wave guide entry), the $g(T)_p$ and $g(T)_q$ waves optically combine by the [8, p. 18] identity: $\sin\alpha + \sin\beta = 2\sin\frac{1}{2}(\alpha+\beta)\cos\frac{1}{2}(\alpha-\beta)$, to form

$$h(T) = g(T)_p + g(T)_q$$
$$= B\left\{\left[\sin\left(\phi_{0_p} + \frac{2\pi\, cT}{\lambda_0} + \frac{2\pi r}{\lambda_0}\int_{\tau=0}^{\tau=T}\omega(\tau)\,d\tau\right)\right] + \left[\sin\left(\phi_{0_q} + \frac{2\pi\, cT}{\lambda_0} - \frac{2\pi r}{\lambda_0}\int_{\tau=0}^{\tau=T}\omega(\tau)\,d\tau\right)\right]\right\}$$
$$= 2B\sin\frac{1}{2}\left(\phi_{0_p} + \phi_{0_q} + \frac{4\pi\, cT}{\lambda_0}\right)\cos\frac{1}{2}\left(\phi_{0_p} - \phi_{0_q} + \frac{4\pi r}{\lambda_0}\int_{\tau=0}^{\tau=T}\omega(\tau)\,d\tau\right) \qquad (13)$$
$$= 2B\sin\left(\frac{\phi_{0_p} + \phi_{0_q}}{2} + \frac{2\pi\, cT}{\lambda_0}\right)\cos\left(\frac{\phi_{0_p} - \phi_{0_q}}{2} + \frac{2\pi r}{\lambda_0}\int_{\tau=0}^{\tau=T}\omega(\tau)\,d\tau\right)$$

Note in the second line of (13) that $2\pi\, cT/\lambda_0$ is present in both $g(T)_p$ and $g(T)_q$, but that these terms cancel when differenced in the cosine argument of the third line in (13). This key point is due to the effect of Relativity that, relative to the rotating gyro, has the independent counter-travelling *p* and *q* waves having the same velocity of light *c*. Without this effect, determination of integrated angular rate from the $h(T)$ signal would not be possible.

The readout photodiode output measures the "sign-less" magnitude of the impinging light wave intensity which can be analytically represented as the normalized power $W(T) = h(T)^2 / B^2$ in the (13) combined beam signal. The development leading to (A-10) of the Appendix shows that (13) for $h(T)$ then obtains for the combined beam power:

$$W(T) = h(T)^2 / B^2 = 1 + \cos\left(\phi_{0_p} - \phi_{0_q} + \frac{4\pi r}{\lambda_0} \int_{\tau=0}^{\tau=T} \omega(\tau)\, d\tau \right) \qquad (14)$$

Eq. (14) defines the readout signal for either a ring laser or fiber optic type optical gyro. The input axis for detection of angular rate $\omega(\tau)$ for each is perpendicular to the plane of the optical wave path (see Fig. 2). The difference in the gyro types depends on values for the $\phi_{0_p} - \phi_{0_q}$ and T terms in (14).

FIBER OPTIC GYROS

A fiber optic gyro (FOG) consists of a circular coil of optical fiber, the ends optically spliced together with fiber-optic couplers, routing near-monochromatic light from a super-luminescent diode (e.g., gallium arsenide) into and out-of the coil [9 pp 186-190; 10; 11]. The concept is depicted in Fig. 3.

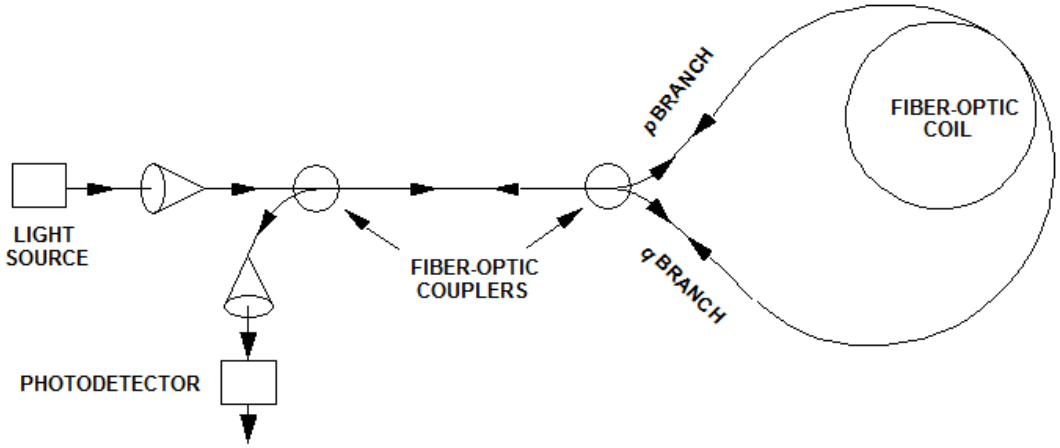

Fig. 3 - Fiber Optic Gyro (FOG) Concept

The light beam from the photo diode light source in Fig. 3 passes through a first coupler, then into the fiber-coil through a second coupler where it splits into two beams, one into the *p* branch, the other into the oppositely directed *q* branch. After traversing the coil, the beams recombine in the second coupler, and are gated through the first coupler to a readout photo detector. Under rotation, the *p* and *q* branch beams experience a relative phase shift, generating a change in the combined beam power illuminating the photo detector. Readout electronics convert the photo detector output into a measurement of angular rotation that created the phase shift. Fig. 3 shows that both the *p* and *q* light beams are generated by the same light source. Thus, *p* and *q* enter the wave path at the same phase, setting $\phi_{0_p} = \phi_{0_q}$, and simplifying(14) to

$$W(T) = 1 + \cos\left(\frac{4\pi r}{\lambda_0} \Delta\theta(T) \right) \qquad \Delta\theta(T) \equiv \int_{\tau=0}^{\tau=T} \omega(\tau)\, d\tau \qquad (15)$$

Closed-Loop FOG Configuration

Eq. (15) illustrates the fundamental difficulty of measuring the scaled angular increment $\Delta\theta(T)$ with the "open-loop" FOG of Fig. 3; the lack of sensitivity in power $W(T)$ for small $\Delta\theta(T)$, the inverse cosine function for $\Delta\theta(T)$ becoming indeterminate at zero input rate, and prone to significant scale factor error (from pickoff output non-linearity characteristics) at non-zero angular increments. In a "closed-loop" FOG, the goal is to create closed-loop bias that maintains $W(T)$ at a known value with high sensitivity for any value of $\Delta\theta(T)$. The applied electrical bias then becomes the measure of $\Delta\theta(T)$ for output under any angular rate. Thus, means must be introduced to enable measuring deviations from the specified $W(T)$ beam power, and providing "closed loop" feedback to maintain $W(T)$ at its desired value under all dynamic angular rate conditions.

For a closed-loop FOG, the equivalent to (15) also derives from (8), but having ϕ_{0_p} and ϕ_{0_q} include additional bias introduced within the fiber coil to enable closed-loop operation and $\Delta\theta(T)$ determination under any input condition. Thus in (8), ϕ_{0_p} would equal $\alpha+\Delta\beta_p$ and ϕ_{0_q} would equal $\alpha+\Delta\beta_q$, where α is the phase of the light beam entering the coil (splitting into *p* and *q* branches as in Fig. 3), and $\Delta\beta_p$, $\Delta\beta_q$ represent additional phase bias intentionally introduced in the *p*, *q* branches within the coil. The closed-loop equivalent to (14) then derives from (8) using the same rationale that led to (14):

$$\begin{aligned} W(T)_m &= 1+\cos\left[\phi_{0_p}-\phi_{0_q}+\frac{4\pi r}{\lambda_0}\int_{\tau=0}^{\tau=T}\omega(\tau)\,d\tau\right] \\ &= 1+\cos\left[\left(\alpha+\Delta\beta_p\right)-\left(\alpha+\Delta\beta_q\right)+\frac{4\pi r}{\lambda_0}\int_{\tau=0}^{\tau=T}\omega(\tau)\,d\tau\right] \\ &= 1+\cos\left(\Delta\beta_p-\Delta\beta_q+\frac{4\pi r}{\lambda_0}\Delta\theta(T)\right) \end{aligned} \qquad (16)$$

Using condensed nomenclature, (16) simplifies to

$$W=1+\cos\left[\Delta\phi+\left(\Delta\beta_p-\Delta\beta_q\right)\right] \qquad \Delta\phi\equiv k_{SF}\,\Delta\theta(T) \qquad k_{SF}\equiv\frac{4\pi r}{\lambda_0} \qquad (17)$$

In modern day FOGs, integrated optics inserts are used to generate the $\Delta\beta_p$ and $\Delta\beta_q$ applied phase shifts in (31), based on the use of active electro-optic crystals that change the index of refraction of light passing through. With this approach, the integrated optics insert is constructed from a crystal of lithium-niobate using titanium strips diffused on the surface to gate light waves through the crystal [9 pp 189-190]. Voltage applied across the crystal changes the index of refraction of light passing through, changing the speed of light waves propagating through the crystal, thereby adding phase shift. For a given applied voltage, the same phase shift

will be added to waves entering from either side of the crystal, i.e., from the *p* or *q* wave directions in a FOG fiber coil. Achieving a net phase difference in (17) relies on the crystal being inserted at one end of the fiber to take advantage of the time interval difference for a *p* wave (for example) to reach the readout photo detector compared to the *q* wave. An example of applying the concept is depicted in Fig. 4, a symmetrical closed-loop FOG version of Fig. 3.

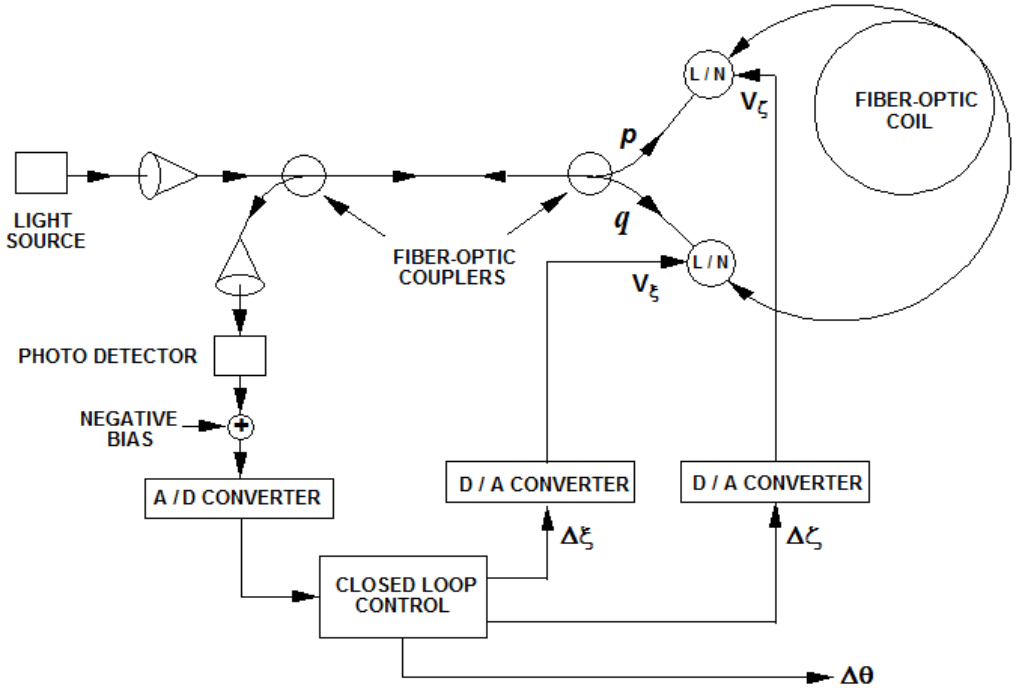

Fig. 4 – Closed-Loop FOG Configuration

Fig. 4 shows how the photo detector output would be applied in feedback fashion through the Closed Loop Control block to generate $\Delta\varsigma$, $\Delta\xi$ phase shifts in the *p*, *q* waves by the V_ς, V_ξ voltages applied to the L/N crystals. In conjunction with generating the $\Delta\varsigma$, $\Delta\xi$ phase shift commands, the Closed Loop Control block in Fig. 4 computes the $\Delta\theta$ angular increment measurement for output. Analog negative bias is also applied in Fig. 3 to reduce A/D converter register round-off error. The associated complex detail is provided in [1].

RING LASER GYROS

A ring laser gyro (RLG) creates two oppositely directed beams of monochromatic light that traverse a closed optical path formed by three or more reflecting mirrors [12, 13]. Beam power losses in an RLG are compensated by amplification within the helium/neon plasma, adding photons at the same wavelength and in phase with returning photons (i.e., through Light Amplification by the Stimulated Emission of Radiation – LASER [12, 13]). The concept is depicted in Fig. 5 for a triangular (3-mirror) gyro configuration.

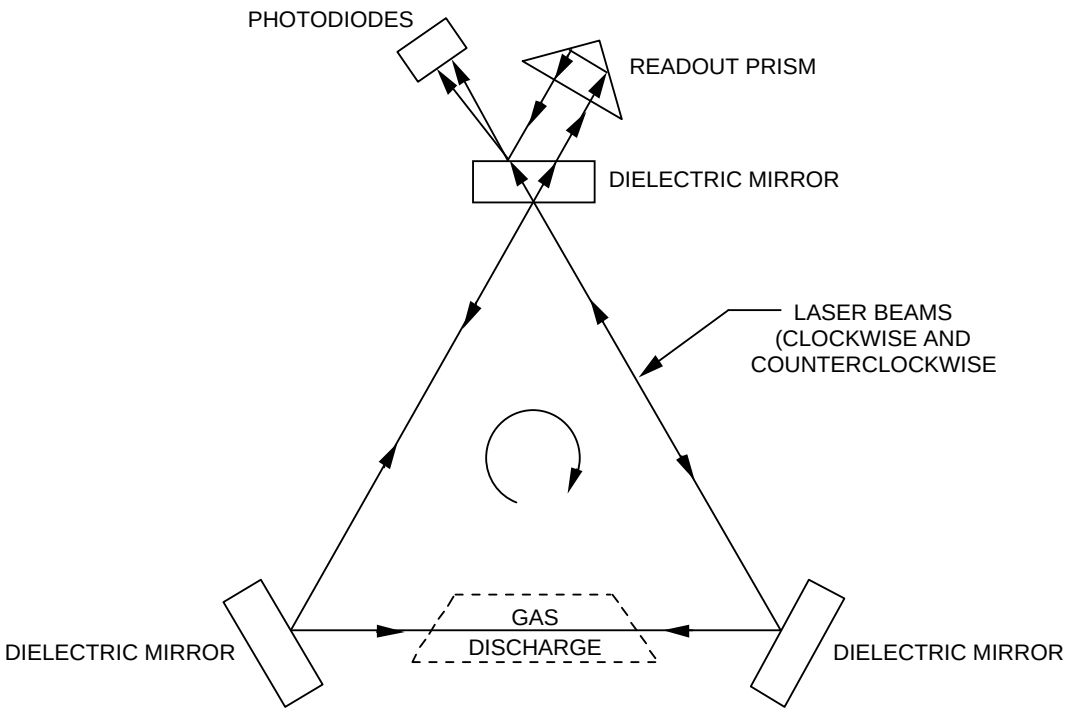

Fig. 5 - Ring Laser Gyro Operating Elements

The reflecting surfaces in Fig. 5 are dielectric mirrors designed to selectively reflect the frequency associated with the particular helium-neon transition being used (typically of 0.63 micron wavelength). A small fraction of each beam escapes the cavity at the readout, one reflected through a corner prism, then recombined with the other on readout photo detectors (mounted in the gyro "readout zone"). The corner prism produces a small angle between the recombining beams, thereby creating optical interference fringes (light and dark bands) on the photo detectors, each illuminated by a different portion of the fringe pattern. The fringe pattern is stationary under zero angular rotation of the cavity. Under cavity rotation, the fringes move across the photo detectors, generating a sinusoidal output at a frequency proportional to the gyro angular rate around its input axis (perpendicular to the plane of the Fig. 3 diagram). Photo detector readout logic converts the sinusoidal output into a digital square wave for each fringe passage. The rise and fall of the square wave edges generate output pulses, each representing an angular rotation through a known angular increment (the gyro output pulse scale factor). Two photo detectors are used, separated from each other by one quarter of a photo-detector-sensed fringe so that resulting sinusoidal outputs are 90 deg phase separated. Comparison between photo detector generated square wave outputs determines the direction of rotation, positive or negative, depending on whether one square wave is leading or lagging the other.

When lasing is achieved, a returning wave at the same point in the waveguide will be in phase with itself, and the total length of the closed wave path will contain an integral number of wavelengths. The result is the equivalent of a continuous beam that begins at laser ignition, continually re-circulating around the mirror-created optical beam path. Based on this operation, the combined beam power Eq. (A-12) of the appendix applies for an RLG when T is replaced by

the equivalent *t*, the current time since laser ignition when *p* and *q* wave photons both originally appeared in the readout zone:

$$W(t)_{\Delta s} = 1 + \cos\left(\phi_{0_p} - \phi_{0_q} + \frac{4\pi \Delta s}{\lambda_0} + \frac{4\pi r}{\lambda_0} \int_{\tau=0}^{\tau=t} \omega(\tau)\, d\tau \right) \qquad (18)$$

Replacing T with t in (18) recognizes that for an RLG, the re-circulating beam path length $L = ct$ continually increases with time t since laser ignition (and light wave creation), hence, measures the continuous integral of angular rate. This contrasts with a FOG in which the path length *L* is fixed, equal to the length of the fiber optic coil, and thus as in (15), measures the integrated angular rate over fixed time interval *T* for light beams to traverse the coil. This fundamental difference is caused by the light source for a FOG being external and independent of the wave path; for an RLG, the "light source" is the stimulated emission process itself within the beam wave path, continually reinforcing the energy in the beams that originated at laser ignition.

The power variation with time effect in (18) shows that the normalized power will cyclically repeat each time $(2r / \lambda_0) \int_{\tau=0}^{\tau=t} \omega(\tau)\, d\tau$ changes by 1, corresponding to an output "scale factor" of $\lambda_0 / 2r$ cycles per $\int_{\tau=0}^{\tau=t} \omega(\tau) d\tau$ integrated angular rate change. For an equilateral triangular RLG with a 2 inch side length (0.167 ft), [8 Eqs. 36 & 63] shows that the inscribed circle radius, hence r in (18), would be $r = 0.167 / 2\tan(\pi / 3) = 0.0482$ ft. For the commonly used RLG wavelength λ_0 of 0.63 micron (2.02 e-6 ft), the gyro scale factor would then be $\lambda_0 / 2r$ = 2.02 e-6 / (2 × 0.0482) = 2.10 e-5 radians = 4.32 arc sec output cycles per radian change in integrated angular rate.

For another power variation effect in (18), consider grouping $\xi \equiv \frac{4\pi \Delta s}{\lambda_0} + \frac{4\pi r}{\lambda_0} \int_{\tau=0}^{\tau=t} \omega(\tau)\, d\tau$ for these terms. For a particular value of ξ, the total phase in the (18) power signal would then be $\phi_{0_p} - \phi_{0_q} + \xi$, and the associated (18) combined beam power would be $W(t) = 1 + \cos\left(\phi_{0_p} - \phi_{0_q} + \xi \right)$. For the particular ξ value we can also rewrite by rearrangement $\frac{4\pi \Delta s}{\lambda_0} = \xi - \frac{4\pi r}{\lambda_0} \int_{\tau=0}^{\tau=t} \omega(\tau)\, d\tau$, whence

$$W(t) = 1 + \cos\left(\phi_{0_p} - \phi_{0_q} + \xi \right) \qquad \Delta s = \frac{\lambda_0 \xi}{4\pi} - r \int_{\tau=0}^{\tau=t} \omega(\tau)\, d\tau \qquad (19)$$

For any particular ξ value, (19) shows that the power $W(t) = 1 + \cos\left(\phi_{0_p} - \phi_{0_q} + \xi \right)$ at moving location Δs will translate across the readout zone as *r* multiplied by the time integral of

angular rate. For a particular ξ value, the derivative of (19) also shows that associated linear rate of the power signal movement across the readout zone would be

$$\frac{d\Delta s}{dt} = - r\ \omega(t) \qquad (20)$$

The $r\ \omega(t)$ term in (20) is the linear velocity relative to non-rotating inertial space, of a point on the gyro at distance *r* from the circular wave path center (point *a* in Fig. 2). Thus, the interferrometrically combined wave would translate at this velocity across the gyro fixed readout zone at location *r*, but by the negative polarity in (20), in a direction opposite from rotation. Then, relative to non-rotating space, the combined beam wave pattern would be stationary, representing a well-known characteristic of RLGs: A standing wave created in non-rotating space within the closed gyro fixed wave path, that is sensed by readout detectors in the rotating gyro as they translate past the standing wave.

CONCLUSIONS

Both fiber optic and ring laser optical gyros (FOGs and RLGs) are designed with closed wave paths to direct monochromatic light waves travelling in both clockwise (cw) and counter-clockwise (ccw) directions. Both gyro types measure the integral of angular rate over the time for light waves to traverse the gyro fixed closed wave path. The angular measurement for both gyros is the phase change generated by the combined cw and ccw beams in the readout zone (interferometrically) for detection on readout photo-diodes. The difference between FOGs and RLGs is how the light source is generated.

The light source in a FOG is a super luminescent diode external to the closed wave path that delivers photons into the wave path for traversal once around the wave path for output measurement. The FOG output then represents the integrated angular rate over the fixed time interval for photons to traverse the gyro fixed wave path.

For an RLG, the "light source" is the laser "stimulated emission" process created within the gyro fixed wave path, continually reinforcing light waves that originated at laser ignition. The result is the equivalent of a light wave that originated at laser ignition, then travelled for readout at any current time over the continually increasing wave path distance. The RLG output measurement thereby represents the integrated angular rate since laser ignition, delivered as fixed integrated angular rate increments created in time by the readout electronics.

APPENDIX – WAVE CONDITIONS UNDER TIME VARYING ANGULAR RATE

The "clockwise" *p* wave and "counterclockwise" *q* wave in an optical gyro first enter the waveguide (defined as point *l*) at past time $\tau = 0$, then combine (at a defined point *m*) in the waveguide "readout zone" at current time $\tau = T$. For a sinusoidal *p* wave, the wave "height" at time $\tau = T$ would be

$$g(T)_p = B \sin \phi(T)_p \qquad (A\text{-}1)$$

where B is the p wave amplitude and $\phi(T)_p$ is the wave front phase $\tau = T$. Note, points l and m are at the same physical location (in the readout zone), but at different times $\tau = 0$ and $\tau = T$.

Now consider two adjacent points i and i_1 along the waveguide between points l and m, point i_1 being an infinitesimally small distance ds_p from i. Further, consider that the distance between points l and i is the distance travelled by the p wave front at the speed of light c over time interval τ, and that the distance travelled by the wave front over infinitesimally small time interval $d\tau$ is ds_p. Then the p wave front phase $\phi(p,i_1)$ at i_1 will relate to $\phi(p,i)$, the phase at point i as

$$\phi(p,i_1) = \phi(p,i) + \frac{2\pi}{\lambda_{p/i}} ds_p = \phi(p,i) + \frac{2\pi}{\lambda_{p/i}} c\, d\tau \qquad \text{(A-2)}$$

and the differential phase difference between points i and i_1 over $d\tau$ will be

$$d\phi(p,i) = \frac{2\pi c}{\lambda_{p/i}} d\tau \qquad \text{(A-3)}$$

Beginning at point l (at $\tau = 0$), the (A-3) differential can be accumulated (integrated) in the waveguide over a succession of i points from point l to point m (at time T):

$$\phi(T)_p = \phi_{0_p} + 2\pi c \int_{\tau=0}^{\tau=T} \frac{d\tau}{\lambda_{p/i}} \qquad \text{(A-4)}$$

where ϕ_{0_p} is the phase at point l wave guide entry, and (as before) $\lambda_{p/i}$ is the wavelength of the p wave front when it reaches point i at time τ, after its traversal from point l along the waveguide since $\tau = 0$. Substituting $\lambda_{p/i}$ from (5) in (A-4) then obtains with (A-1)

$$\phi(T)_p = \phi_{0_p} + \frac{2\pi\, cT}{\lambda_0} + \frac{2\pi r}{\lambda_0} \int_{\tau=0}^{\tau=T} \omega(\tau)\, d\tau \qquad g(T)_p = B \sin \phi(T)_p \qquad \text{(A-5)}$$

In (A-5), angular rate ω time dependence has now been more clearly delineated as $\omega(\tau)$. For the q wave, the equivalent of (A-1) to (A-5) would be

$$\phi(T)_q = \phi_{0_q} + \frac{2\pi\, cT}{\lambda_0} - \frac{2\pi r}{\lambda_0} \int_{\tau=0}^{\tau=T} \omega(\tau)\, d\tau \qquad g(T)_q = B \sin \phi(T)_q \qquad \text{(A-6)}$$

In the readout zone at time interval T (since wave guide entry), the $g(T)_p$ and $g(T)_q$ wave fronts in (A-5) and (A-6) optically combine as in (13) of the main text to form

$$h(T) = g(T)_p + g(T)_q = 2B\sin\left(\frac{\phi_{0_p} + \phi_{0_q}}{2} + \frac{2\pi cT}{\lambda_0}\right)\cos\left(\frac{\phi_{0_p} - \phi_{0_q}}{2} + \frac{2\pi r}{\lambda_0}\int_{\tau=0}^{\tau=T}\omega(\tau)\,d\tau\right) \quad \text{(A-7)}$$

In general, the physical readout width of a photodiode in the readout zone will be small but finite. Thus, the wave front being sensed will also exist at small time interval Δt from T for which (A-7) becomes

$$h(T+\Delta t) = g(T+\Delta t)_p + g(T+\Delta t)_q \quad \text{(A-8)}$$
$$= 2B\sin\left(\frac{2\pi c\Delta t}{\lambda_0} + \frac{\phi_{0_p} + \phi_{0_q}}{2} + \frac{2\pi cT}{\lambda_0}\right)\cos\left(\frac{\phi_{0_p} - \phi_{0_q}}{2} + \frac{2\pi r}{\lambda_0}\int_{\tau=0}^{\tau=T+\Delta t}\omega(\tau)\,d\tau\right)$$

The readout photodiode output measures the magnitude of the impinging light wave intensity which can be analytically represented as the normalized power $W(T+\Delta t) = h(T+\Delta t)^2 / B^2$ in the (A-8) combined beam signal. Substituting (A-8) for $h(T+\Delta t)$, using the [8, p. 18] identities: $\sin^2\alpha = \frac{1}{2}(1-\cos 2\alpha)$ and $\cos^2\beta = \frac{1}{2}(1+\cos 2\beta)$, then obtains

$$W(T+\Delta t) = h(T)^2 / B^2$$
$$= 4\sin^2\left(\frac{2\pi c\Delta t}{\lambda_0} + \frac{\phi_{0_p} + \phi_{0_q}}{2} + \frac{2\pi cT}{\lambda_0}\right)\cos^2\left(\frac{\phi_{0_p} - \phi_{0_q}}{2} + \frac{2\pi r}{\lambda_0}\int_{\tau=0}^{\tau=T+\Delta t}\omega(\tau)\,d\tau\right)$$
$$= \left[1-\cos\left(\frac{4\pi c\Delta t}{\lambda_0} + \phi_{0_p} + \phi_{0_q} + \frac{4\pi cT}{\lambda_0}\right)\right]\left[1+\cos\left(\phi_{0_p} - \phi_{0_q} + \frac{4\pi r}{\lambda_0}\int_{\tau=0}^{\tau=T+\Delta t}\omega(\tau)\,d\tau\right)\right] \quad \text{(A-9)}$$
$$\approx \left[1-\cos\left(\frac{4\pi c\Delta t}{\lambda_0} + \phi_{0_p} + \phi_{0_q} + \frac{4\pi cT}{\lambda_0}\right)\right]\left[1+\cos\left(\phi_{0_p} - \phi_{0_q} + \frac{4\pi r}{\lambda_0}\int_{\tau=0}^{\tau=T}\omega(\tau)\,d\tau\right)\right]$$

The $\frac{4\pi c\Delta t}{\lambda_0}$ term in the first (A-9) cosine argument creates a high frequency modulation on the second bracketed term of $2c / \lambda_0$ hertz. For a typical optical RLG beam wavelength λ_0 of 0.63 microns, the $2c / \lambda_0$ hertz modulation frequency is high enough (2 × 3.0e8 / 0.63e-6 = 9.52 e14 Hz) to be eliminated through attenuation in the photo-detector/readout electronics. Thus, (A-9) reduces to the simpler form

$$W(T) = 1+\cos\left(\phi_{0_p} - \phi_{0_q} + \frac{4\pi r}{\lambda_0}\int_{\tau=0}^{\tau=T}\omega(\tau)\,d\tau\right) \quad \text{(A-10)}$$

Eq. (A-10) can also be extended for another point in the readout zone at small distance Δs from point m (for which (A-10) was derived). The time T phase for the p wave at this point would be advanced from the (A-5) value by the Δs equivalent distance in wavelength fraction

$2\pi\Delta s/\lambda_0$. The same would be true for the *q* wave at time *T* except the phase would be reduced from (A-6) due to its opposite *q* travel direction. Thus, at Δs from *m*, the equivalent to (A-5) and (A-6) at time *T* would be

$$\phi(T)_{p+\Delta s} = \phi_{0_p} + \frac{2\pi\, cT}{\lambda_0} + \frac{2\pi\Delta s}{\lambda_0} + \frac{2\pi r}{\lambda_0}\int_{\tau=0}^{\tau=T}\omega(\tau)\,d\tau \qquad g(T)_{p+\Delta s} = B\sin\phi(T)_{p+\Delta s}$$

$$\phi(T)_{q-\Delta s} = \phi_{0_{q-\Delta s}} + \frac{2\pi\, cT}{\lambda_0} - \frac{2\pi\Delta s}{\lambda_0} - \frac{2\pi r}{\lambda_0}\int_{\tau=0}^{\tau=T}\omega(\tau)\,d\tau \qquad g(T)_{q-\Delta s} = B\sin\phi(T)_{q-\Delta s} \tag{A-11}$$

where $p+\Delta s$ and $q-\Delta s$ identify *p* and *q* parameter at distance Δs from *m*. Carrying out the same development on (A-11) that led from (A-5) – (A-6) to (A-10) then finds for $W(T)_{\Delta s}$, the combined beam power at distance Δs from *m*

$$W(T)_{\Delta s} = 1+\cos\left(\phi_{0_p} - \phi_{0_q} + \frac{4\pi\Delta s}{\lambda_0} + \frac{4\pi r}{\lambda_0}\int_{\tau=0}^{\tau=T}\omega(\tau)\,d\tau\right) \tag{A-12}$$

REFERENCES

[1] Savage, P. G., "Analytical Description of Optical Gyros", SAI WBN-14024, Apr 23, 2019, Updated (November 6, 2022 and March 15, 2024), free access available at www.strapdownassociates.com.

[2] Savage, P. G., "Simplified Description Of Optical Gyros – A Rigorous Analytical Development Without Vector Calculus", SAI WBN-14027, May 23, 2020, Updated April 8, 2024), free access available at www.strapdownassociates.com.

[3] Einstein, A., *Relativity, The Special and the General Theory*, 1961, The Estate of Albert Einstein.

[4] Born, Max, *Einstein's Theory of Relativity*, Dover Publications, Inc., New York.

[5] Savage, P. G., "Differential Kinematics Of Point-To-Point Relativity", SAI WBN-14021**,** March 11, 2018, free access available at www.strapdownassociates.com.

[6] Halfman, Robert L., *Dynamics: Systems, Variational Methods, Relativity, Volume II*, Addison-Wesley, 1962.

[7] Savage, P. G., "Differential Point-To-Point Relativity In Rotating Coordinates", SAI WBN-14022, May 28, 2018, free access available at www.strapdownassociates.com.

[8] Burington, R. S., *Handbook Of Mathematical Tables And Formulas*, R. S. Burington, 1933 – 1948, Handbook Publishers, Inc. Sandusky, OH

[9] Lawrence, A., *Modern Inertial Technology*, Springer-Verlag 1993.

[10] Lefevre, C. L.., “Application Of The Sagnac Effect In The Interferometric Fiber-Optic Gyroscope”, Paper 7, *Optical Gyros And their Applications*, NATO RTO-AG-339, May 1999.

[11] Ezekiel, S. and Arditty, H.J., ed. *Fiber Optic Rotation Sensors and Related Technologies*, Springer-Verlag, Berlin/Heidelberg/New York, 1982.

[12] Killpatrick, Joseph, "The Laser Gyro", IEEE Spectrum, Oct. 1967.

[13] Aronowitz, F., “Fundamentals of the Ring Laser Gyro”, Paper 3., *Optical Gyros And Their Applications*, NATO RTO-AG-339, May 1999.